A Three-Dimensional Model of Lake Ontario's Summer Circulation I. Comparison with Observations

JOHN R. BENNETT

Department of Earth and Planetary Sciences, Massachusetts Institute of Technology, Cambridge 02139

(Manuscript received 11 October 1976, in revised form 4 April 1977)

ABSTRACT

Observations of Lake Ontario during the International Field Year for the Great Lakes are used to develop a three-dimensional numerical model for calculating temperature and current. The model has a variable grid resolution and a horizontal smoothing which filters out small-scale vertical motion caused by truncation error but has little effect on the strong currents of the coastal boundary layer. Resolution of the shore zones and reduced horizontal smoothing improve simulation of both long-term mean flow and current reversals due to low-frequency waves.

1. Introduction

A major reason that verification of lake circulation theories has been difficult is lack of observations. It is difficult to find lakes for which both the circulation and the forcing are known well enough to allow the separation of mathematical and physical deficiencies. At present Lake Ontario is one of the best because of the data collected during the 1972 International Field Year for the Great Lakes. This paper uses some of these data to develop a three-dimensional model of the lake's circulation. The major result of this work is that the mathematical deficiencies are the most important; I found that it is easier to improve the model by resolving the coastal zone and lowering friction than by varying the turbulence formulation or the atmospheric forcing.

By experimenting with a uniform grid version of the model, I was able to isolate two observations which it cannot explain. The first is that the mean flow during mid-summer near the north shore is toward the west—opposite to the wind. The second is a large depression of the thermocline along the north shore and a strong current reversal due to an internal Kelvin wave. Since the model gives results similar to those of Simons (1974, 1975, 1976) when similar forcing and coefficients are used it is logical to look for either a physical mechanism not allowed in the model or for a different numerical method.

Several nonlinear mechanisms have been proposed to explain the flow against the wind:

1) Emery and Csanady (1973) suggested that over cold upwelled water the reduced wind stress leads to a cyclonic stress curl.

2) Wunsch (1973) showed that the Lagrange drift of internal Kelvin waves yields a cyclonic surface circulation.

3) Bennett (1975a) showed that wind-driven currents tend to be stronger at a downwelling shore because the lake static stability is stronger there.

4) Csanady (1975) showed that inertial accelerations in the surface Ekman layer accelerate the shore water to the right of the wind.

The main objection to the Emery and Csanady mechanism is that a cyclonic wind stress curl does not show up in the air; Ching (1974) concluded from an analysis of wind over Lake Ontario that in early summer the surface stress over Lake Ontario is slightly anticyclonic; my own analysis confirms his result. This is reasonable since the lake is colder than the surrounding land and should generate a local high-pressure center.

The Wunsch theory only applies to surface or bottom circulation of particle motion. It predicts that at intermediate depths, particles would drift anticyclonically and that a fixed instrument would not measure a mean flow at any depth. However, the circulation is cyclonic at all levels measured by fixed current meters (Pickett and Richards, 1975).

Comparison of the Bennett and Csanady mechanisms with a cross section model showed that both could possibly be important but that the inertial accelerations tend to be compensated by bottom friction (Bennett, 1974, 1975b). Only when the wind is strong are current speeds much higher at the downwelling shore; even then the vertically averaged flow was little affected. For the time-averaged flow, therefore, it should not be necessary to include the inertial

terms. In the analogous case of an equatorial ocean inertial accelerations are usually considered to be more important (Gill, 1975), because the water is so deep that bottom friction is negligible.

Because these nonlinear effects are not very large and because the empirical model of Bennett and Lindstrom (1977) indicated that large decay times were necessary, I was also trying to improve the model's resolution of the coastal zone and to run it with lower values of friction. These changes improve the simulation of both the mean flow on the north shore and the Kelvin wave episode. It is this fact that I want to communicate here. The reasons for this improvement will be examined in more detail in Part 2.

While the model is similar to that of Simons, it differs in several technical aspects and, more importantly, in verification strategies. Simons used the lakewide current meter array and water level recorders as his primary verification. His model therefore predicts water level explicitly using a free surface and has a uniform grid resolution. The present model was designed to use the nearshore coastal chain data and the long-term temperature trends for its primary verification. Consequently, it uses the rigid lid approximation and has increased resolution near the coast.

The major difference in the numerical methods is that Simons defines both horizontal velocity components at the same point, whereas I do not. This was done partly to avoid the lattice dispersion problem for gravity waves and partly to avoid duplicating Simons' work. The numerical model is designed so that for linear internal waves it is the same as the method of Platzman (1972). Averaging of the Coriolis force was needed because the velocity components are at different grid points causing an effect similar to lattice dispersion. In Platzman's work this is not very important since for the external gravity modes he studied, rotation is only important for scales larger than the grid size. To compensate for some of this truncation error I smooth the divergence of the velocity field. This smoothing corresponds to a horizontal "bulk viscosity." A similar formulation was developed by Sadourney (1972, 1973) for the initialization of numerical weather prediction models.

The model is described in Section 2. Section 3 presents a summary of the shortcomings of the uniform

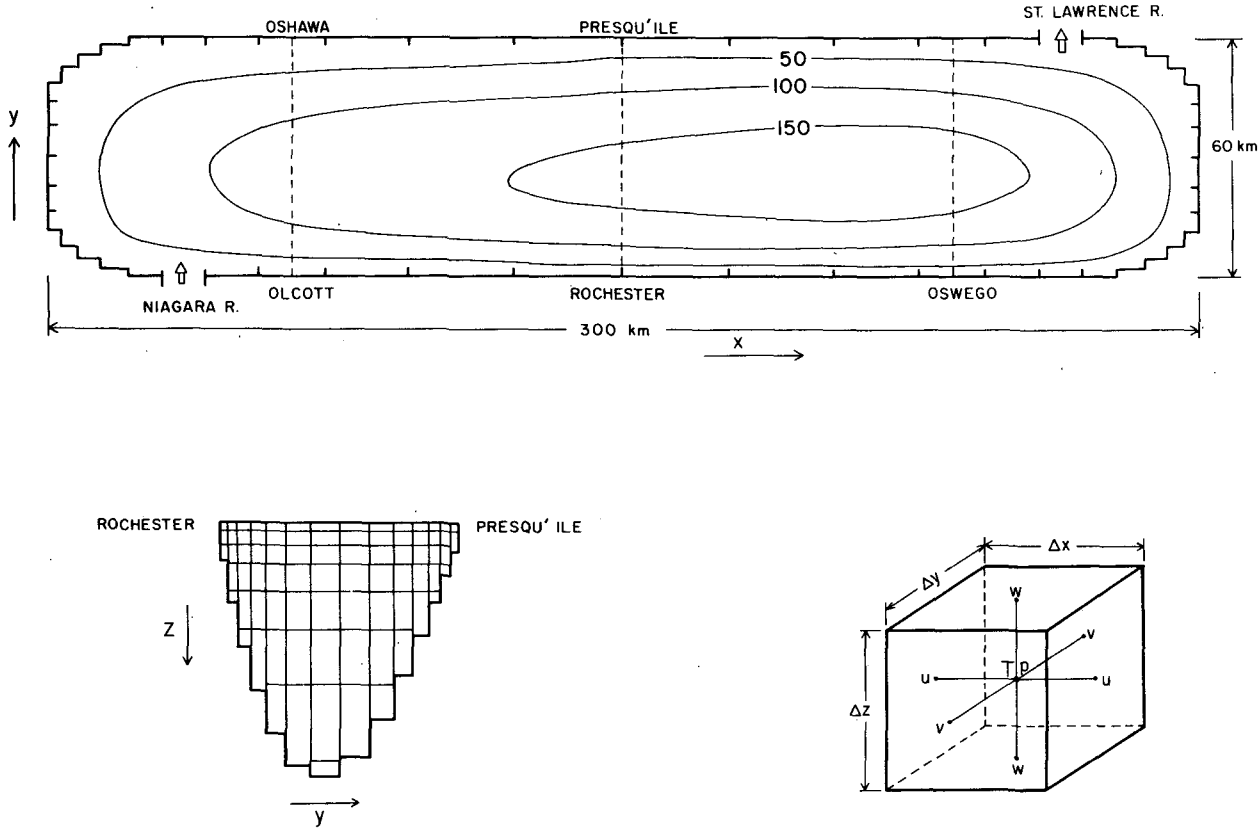

FIG. 1. Finite-difference grid for a three-dimensional model of Lake Ontario. The depth contours are in meters.

grid version and the logic which lead to the improvements. Section 4 gives an analysis of the differences between two variable grid cases, one with friction comparable to that used in the earlier version and in the Simons model and the other with a lower value.

2. The model

The model's physical approximations are as follows:

1) Hydrostatic: vertical accelerations are neglected.
2) Boussinesq: density variations are neglected except where they influence buoyancy.
3) f-plane: the Coriolis parameter is assumed constant and Cartesian coordinates are used.
4) The density is approximated by a quadratic function of temperature.
5) The surface is treated as a rigid lid.
6) Advection of momentum is neglected.
7) Friction is parameterized by a vertical eddy viscosity.
8) Diffusion of heat is parameterized by an eddy diffusivity.

Using the notation in the Appendix, the equations are

$$\frac{\partial u}{\partial t}=fv-\frac{1}{\rho_0}\frac{\partial p_s}{\partial x}-\frac{1}{\rho_0}\frac{\partial p}{\partial x}+A\frac{\partial^2 u}{\partial z^2}, \tag{1}$$

$$\frac{\partial v}{\partial t}=-fu-\frac{1}{\rho_0}\frac{\partial p_s}{\partial y}-\frac{1}{\rho_0}\frac{\partial p}{\partial y}+A\frac{\partial^2 v}{\partial z^2}, \tag{2}$$

$$\frac{\partial}{\partial t}(L\psi)=-f\left(\frac{\partial\psi}{\partial x}\frac{\partial h^{-1}}{\partial y}-\frac{\partial\psi}{\partial y}\frac{\partial h^{-1}}{\partial x}\right)$$

$$-\frac{\partial}{\partial y}\overline{\left[-\frac{1}{\rho_0}\frac{\partial p}{\partial x}+A\frac{\partial^2 u}{\partial z^2}\right]}^{z}+\frac{\partial}{\partial x}\overline{\left[-\frac{1}{\rho_0}\frac{\partial p}{\partial y}+A\frac{\partial^2 v}{\partial z^2}\right]}^{z}, \tag{3}$$

$$\frac{\partial T}{\partial t}=-\frac{\partial(uT)}{\partial x}-\frac{\partial(vT)}{\partial y}-\frac{\partial}{\partial z}\left(wT-K\frac{\partial T}{\partial z}\right), \tag{4}$$

$$\frac{\partial w}{\partial z}=-\frac{\partial u}{\partial x}-\frac{\partial v}{\partial y}, \tag{5}$$

$$b=-6.6\times10^{-3}(T-4)^2, \tag{6}$$

$$p=\int_0^z b\,dz. \tag{7}$$

Eqs. (1) and (2) are momentum equations for the two components of horizontal velocity, (3) is the vorticity equation for the vertically averaged velocity, (4) the thermodynamic energy equation, (5) the incompressibility condition, (6) an approximate equation of state for fresh water and (7) the definition of p.

At the boundaries the normal velocity component is zero except at inflow or outflow points. At the surface the heat flux and shear stress are specified. At the bottom the heat flux is zero and the shear stress is computed with either a linear or quadratic bottom drag law.

Fig. 1 illustrates the finite-difference grid. The basic unit of the grid is a box with a temperature-pressure value at the center and the normal velocity components on the six faces. The streamfunction is a two-dimensional field defined at the corners of the box. The boxes are spaced in a rectangular grid which can be stretched in any of the three dimensions. The horizontal outline of the lake can be approximated by eliminating some boxes; here only the corner points are eliminated. As illustrated by the Rochester-Presqu'ile cross section, the bottom topography is approximated by varying the number of boxes in a column and the thickness of the bottom one.

All the spatial derivatives are approximated by centered differences. The algorithm for advancing the variables forward one time step has six steps:

1) Make an initial estimate (u^*, v^*) of the horizontal velocity components by ignoring the surface pressure gradient:

$$u^*=u^n-\frac{\Delta t}{\rho_0}\frac{\partial p^n}{\partial x}+f\Delta t v^n+A\Delta t\frac{\partial^2 u^n}{\partial z^2}, \tag{8}$$

$$v^*=v^n-\frac{\Delta t}{\rho_0}\frac{\partial p^n}{\partial y}-f\Delta t u^*+A\Delta t\frac{\partial^2 v^n}{\partial z^2}. \tag{9}$$

2) Predict the new value of the streamfunction ψ^{n+1} using some of the terms from the right-hand side of (8) and (9):

$$\frac{L\psi^{n+1}-L\psi^n}{\Delta t}=\frac{f}{2}\left[\frac{\partial h^{-1}}{\partial x}\left(\frac{\partial\psi^{n+1}}{\partial y}+\frac{\partial\psi^n}{\partial y}\right)-\frac{\partial h^{-1}}{\partial y}\left(\frac{\partial\psi^{n+1}}{\partial x}+\frac{\partial\psi^n}{\partial x}\right)\right]$$
$$+\frac{\partial}{\partial y}\overline{\left[-\frac{1}{\rho_0}\frac{\partial p^n}{\partial x}+A\frac{\partial^2 u^*}{\partial z^2}\right]}^{z}$$
$$-\frac{\partial}{\partial x}\overline{\left[-\frac{1}{\rho_0}\frac{\partial p^n}{\partial y}+A\frac{\partial^2 v^n}{\partial z^2}\right]}^{z}. \tag{10}$$

The rotational term is treated differently from the pressure gradient and friction terms here so that errors due to averaging the Coriolis force in the momentum equation do not influence the vertically integrated flow. It is also treated implicitly; this is not done because of the time step limitation for topographic waves but because it is the simplest neutrally stable method using two time levels. The values of

ψ^{n+1} are computed from this equation by Duftor-Frankel relaxation.

3) The horizontal velocity components are corrected for the neglect of the surface pressure gradient by making them consistent with the new streamfunction:

$$u^{n+1}=u^*-\overline{u^*}^z-\frac{1}{h}\frac{\partial\psi^{n+1}}{\partial y}, \tag{11}$$

$$v^{n+1}=v^*-\overline{v^*}^z+\frac{1}{h}\frac{\partial\psi^{n+1}}{\partial x}. \tag{12}$$

4) The new vertical motion is computed by integrating (4):

$$\frac{\partial w^{n+1}}{\partial z}=-\frac{\partial u^{n+1}}{\partial x}-\frac{\partial v^{n+1}}{\partial y}. \tag{13}$$

This integration can begin at either the top or bottom; (11) and (12) ensure that w is zero at both.

5) The new temperature is computed from (5) by using the Adams-Bashforth method for the advective terms and a forward time step for the diffusive terms.

6) The new pressure is computed from (6) and (7).

At this point the horizontal smoothing is incorporated by adding a term proportional to the horizontal divergence to the pressure, i.e.,

$$\frac{p^{n+1}}{\rho_0}=\int_0^z b^{n+1}dz-A_x\left(\frac{\partial u^{n+1}}{\partial x}+\frac{\partial v^{n+1}}{\partial y}\right). \tag{14}$$

This is equivalent to adding viscosity terms to (1) and (2) of the form

$$\frac{\partial}{\partial x}\left[A_x\left(\frac{\partial u}{\partial x}+\frac{\partial v}{\partial y}\right)\right], \tag{15}$$

$$\frac{\partial}{\partial y}\left[A_x\left(\frac{\partial u}{\partial x}+\frac{\partial v}{\partial y}\right)\right]. \tag{16}$$

The energy dissipation is

$$A_x\left(\frac{\partial u}{\partial x}+\frac{\partial v}{\partial y}\right)^2. \tag{17}$$

In analogy with compressible flow A_x is a horizontal bulk viscosity. This is necessary because the averaging of the Coriolis terms underestimates the effect of rotation in limiting vertical motion. This can be illustrated by the finite-difference solution to the following steady-state momentum equations:

$$-fv'=0, \tag{18}$$

$$fu'=0. \tag{19}$$

These equations apply to the vertical shear in regions where stratification and friction are small. The solution is $u'=v'=0$, implying that the horizontal current is independent of depth. However, the finite-difference equations

$$-f\overline{v'}^{xy}=0, \tag{20}$$

$$f\overline{u'}^{xy}=0, \tag{21}$$

admit any solution for which the sum of any four adjacent points is zero. Since this small-scale motion behaves as if rotation is zero any forcing at this scale will give a response large enough for friction or stratification to balance the forcing. Smoothing this small-scale motion with a Laplacian viscosity filters out all small-scale motions including physically realistic boundary layers and coastal trapped low-frequency waves. However, the horizontal bulk viscosity filters out only the small-scale motion with large horizontal divergence. Since for low-frequency waves most of the energy is in nondivergent motion they are damped only slightly. To make this viscosity term the same order as the truncation error caused by averaging the Coriolis force over four points requires A_x to be proportional to f and the square of the grid size. Here the formula

$$A_x=0.25f\min^2(\Delta X,\Delta Y) \tag{22}$$

was used.

3. Uniform grid experiments

This version differs from the improved one in that the horizontal grid size is 5 km everywhere and it includes more realistic variations in the lake outline and depth. The standard form of lateral eddy viscosity with a value of $A_x=10^6$ cm^2 s^{-1} was used. In addition, variations in the wind stress field, inertial accelerations and stability dependent diffusion coefficients were included in some cases.

The simulation presented here begins on 1 July 1972. The initial temperature field was interpolated from a temperature cruise of 26–28 June and the currents are zero. The vertical eddy viscosity and thermal diffusivity were computed from a variation of the Munk-Anderson formulas:

$$A=100\left|\frac{\tau}{\rho_0}\right|\left(\frac{1}{1+10\mathrm{Ri}}\right)^{\frac{1}{2}},$$

$$K=100\left|\frac{\tau}{\rho_0}\right|\left[\frac{1}{1+\frac{10}{3}\mathrm{Ri}}\right]^{\frac{1}{2}},$$

$$\mathrm{Ri}=\frac{g}{\rho_0}\frac{\partial\rho}{\partial z}\Big/\left|\frac{\partial \mathbf{V}}{\partial z}\right|^2.$$

The bottom stress was computed from

$$\frac{\tau_b}{\rho_0}=0.002|\mathbf{V}_b|\mathbf{V}_b.$$

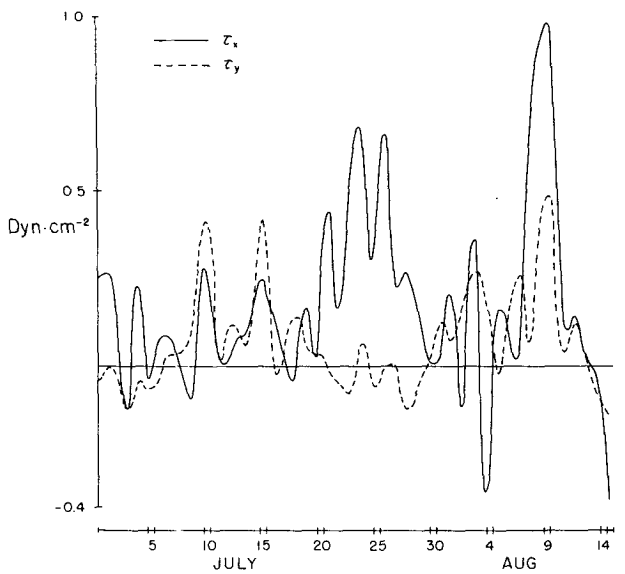

FIG. 2. Wind stress on Lake Ontario 1 July–15 August 1972, computed from wind at a mid-lake buoy and a wind stress coefficient of 1.5×10^{-6}.

The wind stress was computed by the method of Simons, i.e., by interpolating the wind from the buoys by a three-station inverse square law and computing the stress from

$$\tau_w = 1.875\times10^{-6}|\mathbf{W}|\mathbf{W}.$$

Here the wind $\mathbf{W}$ is measured in centimeters per second and the coefficient includes the air-water density ratio. For the case discussed here only the lake average of the stress was used. The surface heat flux, estimated from the observed heat content change, was from the air to the water at 324 cal cm^{-2} day^{-1} (157 W m^{-2}).

A smoothed version of the wind stress is given in Fig. 2. This was calculated by F. C. Elder of the Canada Centre for Inland Waters from a single buoy (IFYGL buoy 10) in the center of the lake but is essentially the same as the lake average. There are two periods of relatively strong stress, 22–26 July and 9–10 August.

I experimented with many combinations of initial conditions, the wind stress field, and the turbulence

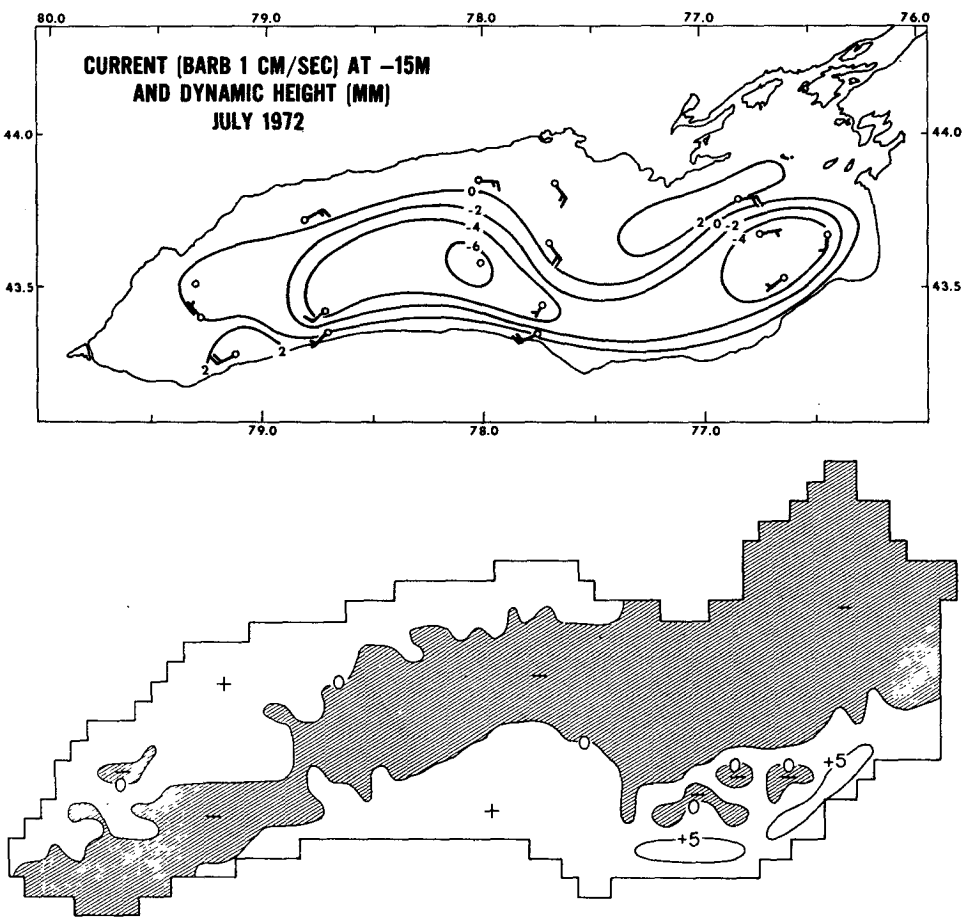

FIG. 3. Lake Ontario current and dynamic height at 15 m depth, 1–31 July 1972 (a) and, eastward component of velocity at 15 m depth, 1–31 July 1972, computed with a 5 km uniform grid numerical model (b).

model and compared the results with several types of data. The first is the lakewide current meter array. Pickett and Richards (1975) provided Fig. 3a, the monthly mean current and dynamic height at 15 m for July 1972. The circulation is dominated by a large cyclonic gyre in geostrophic equilibrium. This is what one would expect in early spring when the shallow shore zones warm up faster than the deep regions. The model-predicted monthly mean eastward component of current (Fig. 3b) shows the correct direction of flow over most of the lake but along the north shore there is a broad band of eastward flow, in the direction of the wind but opposite the observed current. There is no evidence for this flow in any of the current meters nearer shore or in the transacts of Csanady and Scott (1974). All of the observations show a mean down-tilt of the thermocline and a westward flow along the north shore. The model shows a mean upwelling of the thermocline and an eastward flow.

The second indication of the model's inadequacy is that it fails to reproduce the observed strength of current reversals and changes in thermocline depth. One striking example of this is illustrated in Fig. 4, which shows the temperature at 20–40 m from a ship cruise of 1–3 August and from the numerical model. The observations show a large depression of the thermocline along the north shore. Csanady and Scott (1974) show that this downwelling originated about a week before along the south shore and propagated around the east end of the lake. The propagation speed, the sharp temperature gradient and associated large current speed ($\sim$30 cm s^{-1}) agree with their internal Kelvin wave model. The numerical model reproduced the original downwelling along the south shore but by this time the temperature gradient is

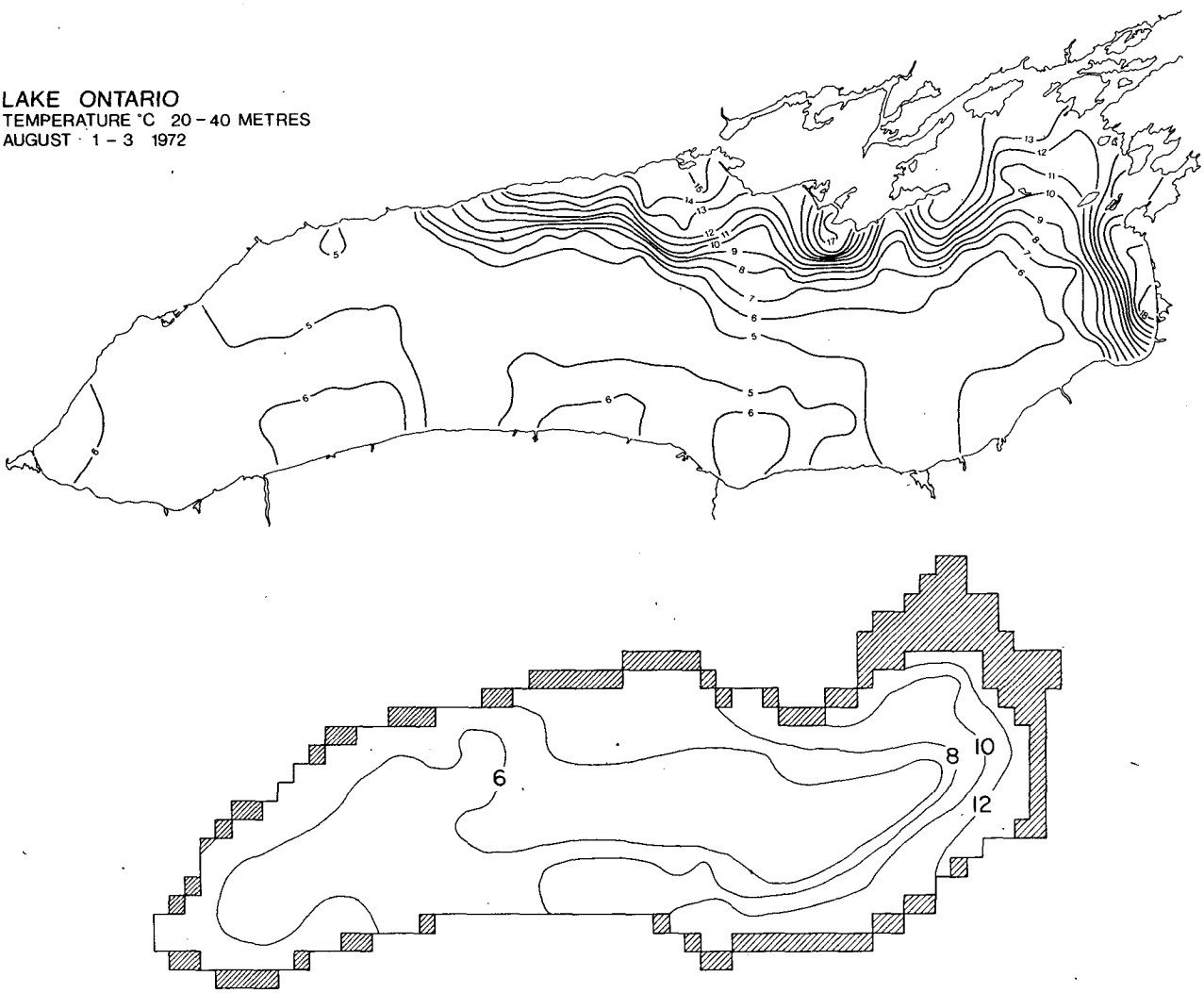

FIG. 4. Temperature at 20–40 m 1–3 August 1972 (a) and at 20–40 m 2 August 1972 computed with a 5 km uniform grid numerical model (b).

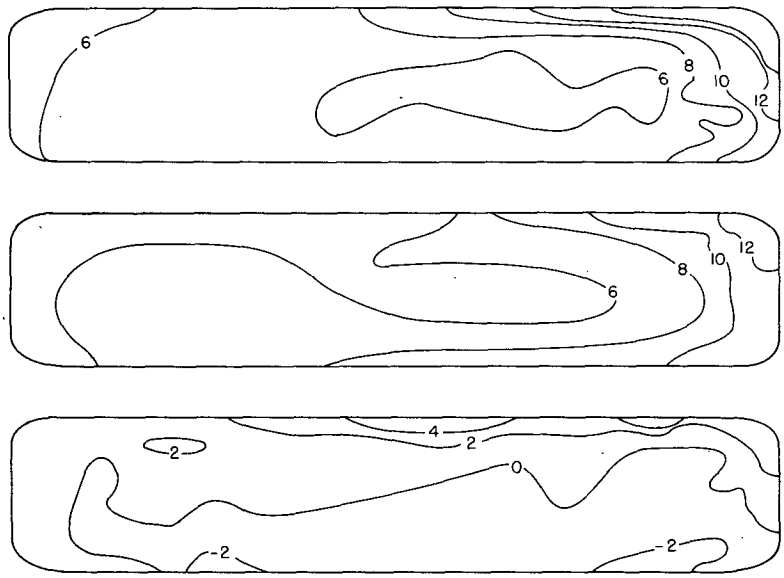

FIG. 5. Temperature at 20–40 m 2–3 August 1972 computed with a vertical eddy viscosity $A = 4$ cm^2 s^{-1} (top), with $A = 32$ cm^2 s^{-1} (middle), and the difference 5a minus 5b (lower).

considerably weaker and the warm water does not extend as far along the north shore as observed.

There are several reasons to expect that lowering friction and resolving the coastal zone would improve the model. First, the internal Kelvin wave, which has an offshore scale comparable to the grid size, would not decay as fast. Second, the spring thermal pattern—warm water at the shore, cold water at the

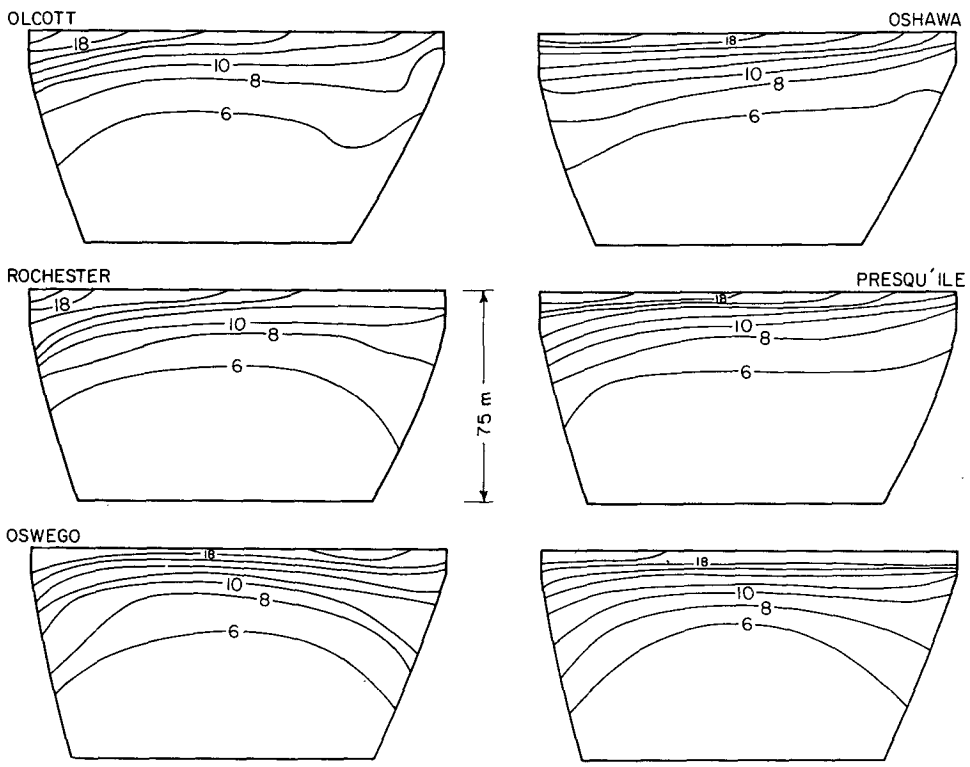

FIG. 6. Temperature 15 July–15 August 1972 at three cross sections of Lake Ontario: left, computed with $A = 4$ cm^2 s^{-1}; right, $A = 32$ cm^2 s^{-1}.

middle and its associated cyclonic flow—would not spin down as fast. Both these effects would decrease the upwelling near the north shore, but the wind's tendency to cause upwelling, however, would not be increased by decreasing friction because the upwelling would be limited to the Ekman flux. In fact, the theory of Birchfield (1972) predicts that when friction is lowered, the Ekman transport is compensated by longshore divergence rather than by upwelling of the deep water.

4. Variable resolution experiments

Since it is difficult to directly compare the old and new models, comparison will be made of two cases of the variable resolution model with different friction formulations. Both use the lateral friction given by (14) and (22), but to simulate the effect of the Laplacian-type smoothing used in the 5 km grid model a larger vertical viscosity and a linear bottom drag were used. The two cases (referred to hereafter as $A=4$ and $A=32$) have the following vertical friction and bottom boundary conditions:

$$A=4\begin{cases} A=4 \text{ cm}^2 \text{ s}^{-1} \\ A\dfrac{\partial v}{\partial z}=0.002|\mathbf{V}|\mathbf{V} \quad \text{at} \quad z=H \end{cases}$$

$$A=32\begin{cases} A=32 \text{ cm}^2 \text{ s}^{-1} \\ A\dfrac{\partial \mathbf{V}}{\partial z}=0.04\mathbf{V} \text{ cm s}^{-1} \quad \text{at} \quad z=H. \end{cases}$$

Both used a constant thermal diffusivity K of 0.25 cm^2 s^{-1}.

For comparison with Fig. 4, Fig. 5 gives the temperature at 20–40 m, 2–3 August for $A=4$, $A=32$ and the difference in temperature between the two cases. As expected, with a lower value of friction, the temperature gradient is much stronger and the warm water extends further to the west.

To analyze the model's ability to simulate the time-averaged flow and temperature structure the two cases were run for 1 July–15 August 1972 and averages were calculated for the observational period 15 July–15 August at the three sections where velocity and temperature were taken (Fig. 1).

The observed mean temperature and eastward component from the north shore is given in Fig. 8. At both Oshawa and Presqu'ile there is a depression of the thermocline and westward flow. The computed mean temperature for this period at the three cross sections is given in Fig. 6; the computed mean eastward component of current is shown in Fig. 7. The low-viscosity case ($A=4$) is on the left and the high-

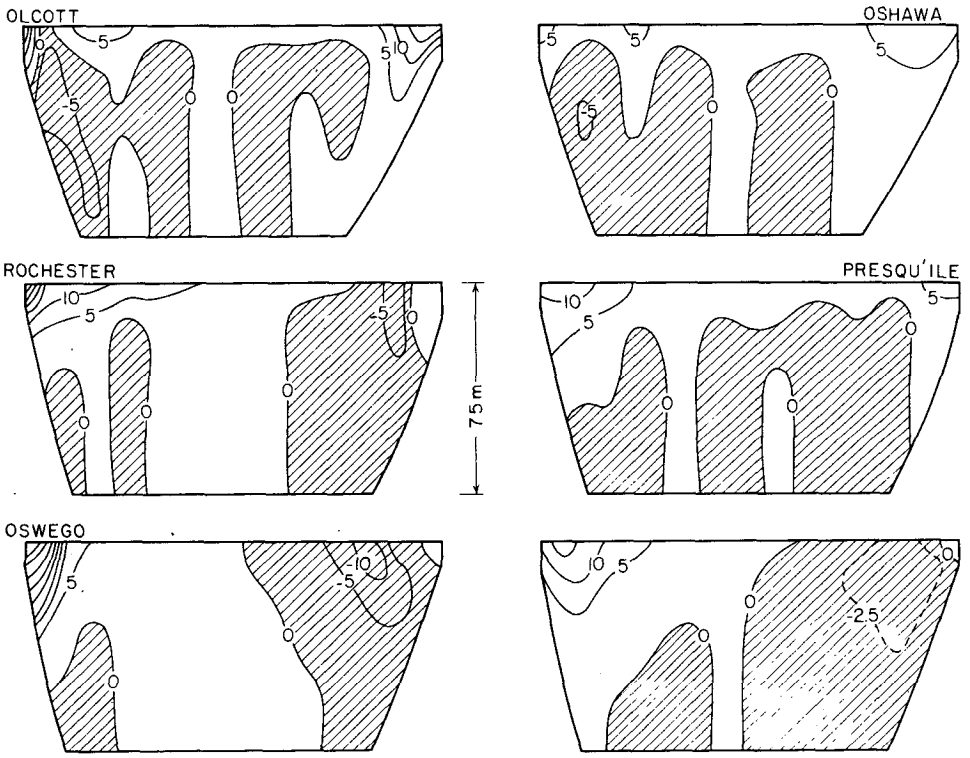

FIG. 7. Eastward component of velocity (cm s^{-1}) 15 July–15 August 1972 at three cross sections of Lake Ontario: left, computed with $A=4$ cm^2 s^{-1}; right, $A=32$ cm^2 s^{-1}.

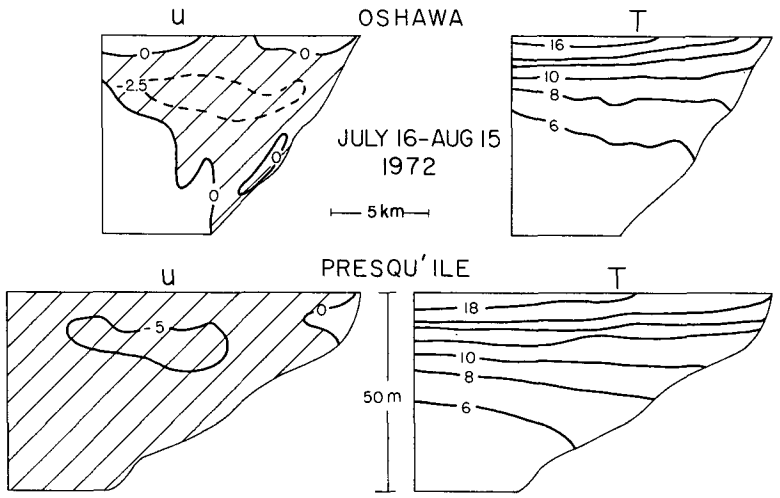

FIG. 8. Eastward velocity and temperature 15 July–15 August 1972 at Oshawa and Presqu'ile observed by Pade and Csanady.

viscosity case ($A=32$) on the right. The major difference between the two cases is that for $A=4$, the upwelling of the thermocline near the north shore is much less than for $A=32$. This is particularly true for the Rochester-Presqu'ile section. In addition the band of westward flow is much nearer to shore for the lower viscosity.

The mean streamfunction for the two model cases and the difference between the two are given in Fig. 9. There is no dramatic difference between the two cases. Both show a large cyclonic gyre in the eastward two-thirds of the lake and an anticyclonic gyre in the western third. This pattern is due to a cyclonic flow superimposed on a two-gyre wind-driven flow. The wind-driven flow in the center is to the right of the mean wind and approximately equal to the Ekman drift. This flow is recirculated around the boundary in a coastal layer. In agreement with Birchfield's theory (1972), the largest longshore transports are to the left of the wind at the upwind and downwind

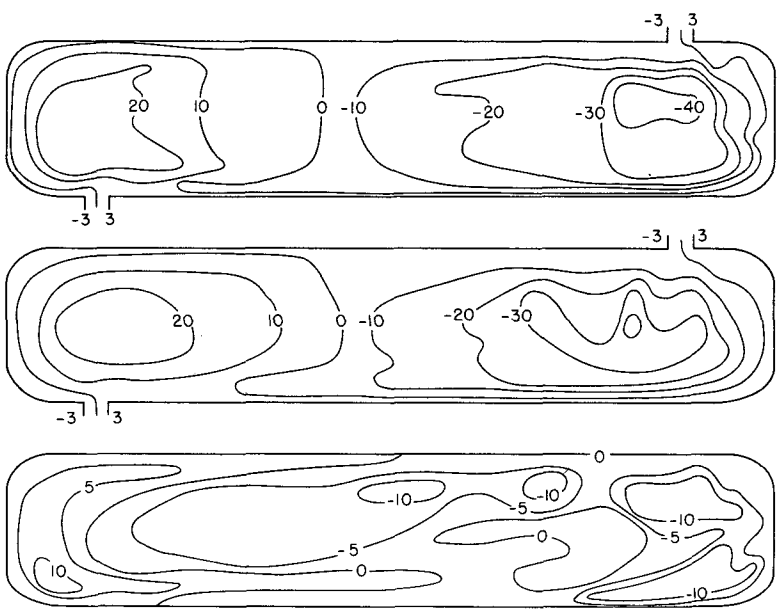

FIG. 9. Streamfunction (10^9 cm^3 s^{-1}) 15 July–15 August 1972 computed with a vertical eddy viscosity $A=4$ cm^2 s^{-1} (top), with $A=32$ cm^2 s^{-1} (middle), and the difference 9a minus 9b (bottom).

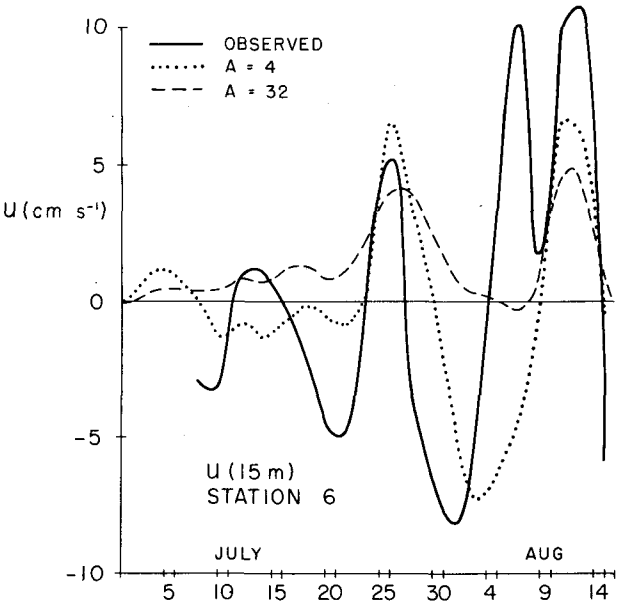

FIG. 10. Eastward velocity at 15 m depth about 10 km south of Oshawa observed and computed with vertical eddy viscosities of 4 and 32 cm² s⁻¹.

shores and for the lower viscosity the coastal layer is thinner. One fact that is not in agreement with the Birchfield theory is that the component of flow to the right of the wind in the center is larger for the high viscosity case than for the low one. This fact is explained by Bennett (1975c) by a model which does not assume the Ekman number is small as Birchfield does.

Finally, Fig. 10 gives the eastward component of velocity at a point about 12 km south of Oshawa and 15 m deep for the two model cases and from the current meter at about 78°50′W, 43°20′N in Fig. 3a. The data used to draw this figure were 2-day averages; the model currents are averages over 2 days and several grid points. For the larger friction, $A=32$, the current accelerates during the two major wind impulses and decays afterward with perhaps a weak reversal. In contrast, both the data and the low-friction model not only give a larger direct response to the wind but a reversal of comparable magnitude.

Acknowledgments. I thank T. J. Simons, G. T. Csanady, J. T. Scott, Dennis Landsberg, R. L. Pickett, F. P. Richards, F. C. Elder, Richard Aselin and G. K. Sato for their comments and data.

This work was supported by the Great Lakes Environmental Research Laboratory of the National Oceanic and Atmospheric Administration under Contract 03-5-022-57 and by a Grant from the Henry L. and Grace Doherty Charitable Foundation, Inc.

APPENDIX

List of Symbols

x, y, z	Cartesian coordinates (z positive downward)
u, v, w	velocity components (w positive downward)
$h(x, y)$	depth of lake
p	pressure minus surface pressure $\left[=\int_0^z b\,dz\right]$
p_s	surface pressure
T	temperature
$b(T)$	buoyancy $\left[=\frac{g(\rho-\rho_0)}{\rho_0}\right]$
ρ_0	density of fresh water at 4°C (1.00000)
ρ	density
$\overline{(\ )}^z$	vertical average operator $\left[=\frac{1}{h}\int_0^h (\ )\,dz\right]$
ψ	streamfunction $\left[\bar{u}^z=-\frac{1}{h}\frac{\partial\psi}{\partial y};\ \bar{v}^z=\frac{1}{h}\frac{\partial\psi}{\partial x}\right]$
L_ψ	vorticity of the vertically averaged flow $\left[=\frac{\partial}{\partial x}\left(\frac{1}{h}\frac{\partial\psi}{\partial x}\right)+\frac{\partial}{\partial y}\left(\frac{1}{h}\frac{\partial\psi}{\partial y}\right)\right]$
K	vertical eddy diffusivity
A	vertical eddy viscosity
τ_w	wind stress

REFERENCES

Bennett, J. R., 1974: On the dynamics of wind-driven lake currents. *J. Phys. Oceanogr.*, **4**, 400–414.

——, 1975a: Another explanation of the observed cyclonic circulation of large lakes. *Limnol. Oceanogr.*, **20**, 108–110.

——, 1975b: Nonlinearity of wind-driven currents. *Proc. Symp. on Modeling of Transport Mechanisms in Oceans and Lakes*, Canada Centre for Inland Waters, Manuscript Rep. Ser. No. 43, Marine Science Directorate, Dept. of Fisheries and the Environment, Ottawa.

——, 1975c: The circulation of large lakes. *Proc. Third Int. Symp. on Upwelling Ecosystems*, Kiel.

——, and E. J. Lindstrom, 1977: A simple model of Lake Ontario's coastal boundary layer. *J. Phys. Oceanogr.*, **7**, 620–625.

Birchfield, G. E., 1972: Theoretical aspects of wind-driven currents in a sea or lake of variable depth with no horizontal mixing. *J. Phys. Oceanogr.*, **2**, 355–366.

Ching, J. K. S., 1974: A study of lake-land breeze circulation over Lake Ontario from IFYGL buoy observations. *Proc. 17th Conf. on Great Lakes Research*, Int. Assoc. Great Lakes Res., 259–268.

Csanady, G. T., 1975: Lateral momentum flux in boundary currents. *J. Phys. Oceanogr.*, **5**, 705–717.

——, and J. T. Scott, 1974: Baroclinic coastal jets in Lake Ontario during IFYGL. *J. Phys. Oceanogr.*, **4**, 524–541.

Emery, K. O., and G. T. Csanady, 1973: Surface circulation of lakes and nearly land-locked seas. *Proc. Nat. Acad. Sci. U.S.*, **70**, 93–97.

Gill, A. E., 1975: Models of equatorial currents. *Numerical*

Models of Ocean Circulation, R. O. Reid, A. R. Robinson and K. Bryan, Eds., Nat. Acad. Sci. U.S., 364 pp.

Pickett, R. L., and F. P. Richards, 1975: Lake Ontario mean temperatures and mean currents in July 1972. *J. Phys. Oceanogr.*, **5**, 775–781.

Platzman, G. W., 1972: Two-dimensional free oscillations in natural basins. *J. Phys. Oceanogr.*, **2**, 117–138.

Sadourney, R., 1972: Approximations en différences finies des équations de Navier-Stokes appliqués à un écoulement géophysique. Thèse de doctoret, University of Paris VI.

——, 1973: Forced geostrophic adjustment in large scale flow. Laboratoire de Meteorologie Dynamique, CNRS, Paris.

Simons, T. J., 1974: Verification of numerical models of Lake Ontario: Part I. Circulation in spring and early summer. *J. Phys. Oceanogr.*, **4**, 507–523.

——, 1975: Verification of numerical models of Lake Ontario. II. Stratified circulations and temperature changes. *J. Phys. Oceanogr.*, **5**, 98–110.

——, 1976: Verification of numerical models of Lake Ontario. III. Long-term heat transports. *J. Phys. Oceanogr.*, **6**, 372–378.

Wunsch, C. I., 1973: On the mean drift in large lakes. *Limnol. Oceanogr.*, **18**, 793–795.